ALUMINUM SUB-MICRON SUPERCONDUCTING HOT-ELECTRON BOLOMETER MIXERS

I.Siddiqi, A. Verevkin, and D.E. Prober
Department of Applied Physics, Yale University, 15 Prospect Street, New Haven, Connecticut 06520-8284

A. Skalare, B.S. Karasik, W.R. McGrath, P. Echternach, and H.G. LeDuc
Center for Space Microelectronics Technology, Jet Propulsion Laboratory,
California Institute of Technology, Pasadena, California 91109

We report on microwave measurements of superconducting aluminum hot-electron bolometers (Al HEBs). Diffusion-cooled Al HEB mixers are ideal candidates for space-borne and terrestrial remote-sensing applications in the Terahertz frequency range since they are predicted to have small local oscillator (LO) power requirements, intermediate frequency (IF) bandwidths $\gtrsim$ 10 GHz, and a noise temperature lower than that of Nb and NbN HEBs.[1] Mixer measurements were made at an LO frequency ~30 GHz LO, with an IF in the range 0.1-7.3 GHz. For T < 0.8 K, a magnetic field H=0.1-0.3T was applied to suppress the superconductivity in the contact pads, and partly in the bridge. For a 0.6 μm long Al HEB, we measure an IF bandwidth of 4 GHz, a conversion efficiency η = -8dB, and a mixer noise temperature $T_m \gtrsim 4$K, DSB ($T_{mixer}=T_{output\ noise}/2\eta$). These results are shown to be in quantitative agreement with simple theoretical predictions.

I. Introduction

Recent studies on Nb and NbN hot-electron bolometer (HEB) mixers have demonstrated that they are excellent candidates for Terahertz spectroscopy applications.[2-4] For Nb HEB mixers, the largest intermediate frequency (IF) bandwidths are obtained for devices much shorter than the inelastic electron-phonon length. These rely on the out-diffusion of hot electrons from the microbridge into cold reservoirs as the dominant mode of energy relaxation.[5] Diffusion-cooled Nb mixers have demonstrated IF bandwidths up to 10 GHz, with the local oscillator (LO) power needed for optimal operation typically ~ tens of nW at Terahertz frequencies. The noise performance of diffusion-cooled Nb devices is excellent, with an achieved receiver noise temperature T_R=1800K, DSB at 2.5THz. [3]

Recently, HEBs employing superconductors with a lower transition temperature than Nb (T_c ~ 6K) have been proposed.[1] The devices studied here are diffusion-cooled HEBs based on Al, with T_c ~ 1.5 to 2.4K. Improvements in mixer performance are predicted because clean Al films have a lower transition temperature and a higher diffusivity D than Nb films.

We present measurements for Al HEB mixers at microwave frequencies. The frequency of the LO source used is ~ 30 GHz. The primary motivation for studying mixing at microwave frequencies is that much of the device physics relevant to THz mixing can be explored with the simpler microwave measurements. Previous microwave studies of Nb HEBs has been useful in this respect.[2]

We present here predictions for mixer performance of Al HEB[1,2] devices. The IF bandwidth of the HEB mixer can be estimated from the thermal time constant τ_{th} of the device. The thermal relaxation rate has a term due to inelastic electron-phonon scattering, and one due to the

"out" diffusion rate -- $\tau_{th}^{-1} = \tau_{e\text{-}ph}^{-1} + \tau_{diff}^{-1}$. In our devices, electron-phonon scattering is negligible, and the thermal time constant is given by the diffusion time[2]

$$\tau_{th} \approx \tau_{diff} = L^2/\pi^2 D, \qquad (1a)$$

and the –3dB intermediate frequency roll-loff is given by:

$$f_{-3dB} = 1/(2\pi\tau_{eff}) = 1/(2\pi\tau_{th}). \quad (1b)$$

L is the length of the bolometer. Eq. (1b) applies when electro-thermal feedback is small, so that $\tau_{eff} = \tau_{th}$. Otherwise τ_{eff} is given by Eq. 5. The conversion efficiency thus drops by a factor of two at IF = f_{-3dB}.

The diffusivity can be expressed as a function of the resistivity by using free electron relations.[12] The mean free path *l* is given by $mv_f/ne^2\rho$, where m is the electron mass, v_f is the Fermi velocity, n is electron concentration, e is the electron charge, and ρ is the resistivity. The diffusion constant is related to the mean free path by $D=v_f\, l\, /3$. Combining these equations gives

$$D = \frac{mv_f^2}{3ne^2\rho}. \qquad (2)$$

For Al, using 1.3×10^8 cm/s for the Fermi velocity and 18.1×10^{22} cm^{-3} for the electron concentration, Eq. (2) reduces to $D[cm^2/s]=114/\rho[\mu\Omega\text{-cm}]$. In Fig. 1, diffusivity data for thin Al films [6-11], including measurements on the films discussed in this work, are presented along with the prediction from Eq. (2). Al HEBs can offer large IF bandwidth.

To maximize the IF bandwidth, or equivalently to minimize the thermal time τ_{th}, the device length is first minimized. Calculations for the order parameter in an N-S-N structure[13,14] indicate that $L_c \sim 2\xi$ is the minimum length for the existence of superconductivity at $T/T_c=0.3$. ξ is the coherence length in the Al microbridge. The order parameter will approach the bulk Ginzburg-Landau value in the middle of the microbridge for devices twice this critical length.[15] Since the coherence length in Al is relatively large, it is possible with current lithographic techniques to make devices a few coherence lengths long. Substituting $L=4\xi$ into Eq. (1a) for the thermal time gives ~ 4.5 ps. The maximum IF bandwidth is thus ~ 35 GHz.

Al HEBs are also promising since the LO power required for operation is predicted to be lower than that of Nb and NbN mixers. The LO power for a diffusion-cooled device is given by[2,16]

$$P_{LO} = 4\mathcal{E}\,(T_c^2 - T^2)/\,R. \qquad (3)$$

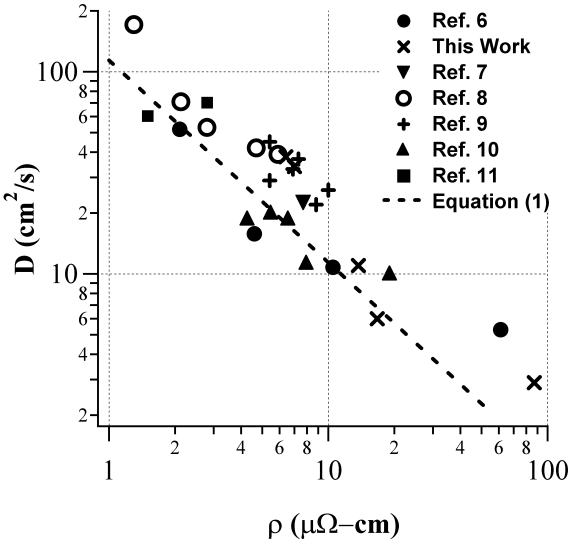

Fig. 1: Diffusivity vs. resistivity for thin Al films with thickness 7-25 nm.

Device	R_n (Ω)	L (μm)	ρ (μΩ-cm)	D (cm^2/s)
A	52	0.6	15	6.0
B	145	0.3	65	2.5
C	260	1.0	36	4.4
D	387	0.6	85	2.9

Table I: Device parameters. Diffusion constant value of devices A and D are measured, while those for B and C are inferred from the resistivity. The device width is 0.1μm. For mixer tests, Tc=1.0K for device A in a magnetic field to 2.4K for device B in zero field.

where $\mathcal{L}$ = 2.45x10-8 Watt-Ohm/K^2 is the Lorenz constant and R the device resistance. At 2.5 THz, for Nb HEBs, P_{LO} ~ 20 nW[3] and P_{LO} ~ 100 nW[17] for NbN phonon-cooled HEBs. In the Al mixer, the critical temperature is approximately 4x smaller than in Nb devices, and thus the LO power should decrease by 16x if the device is operated at a bath temperature well below the critical temperature. The LO power dissipated in the mixer in Al should be ~ 0.2 nW based on scaling of the data obtained for Nb at 20 GHz[2], and ~2nW for THz operation.[18,26]

Though HEB mixer theories for noise are currently under discussion, we discuss here two main thermal noise sources: thermal fluctuation noise and Johnson noise. The contribution of thermal fluctuation noise to the total device noise is proportional to the critical temperature[19], and should thus be smaller in Al devices than in Nb ones. Lowering the T_c of the HEB will similarly result in a decrease of the Johnson noise. Quantum noise, however, must also be considered. A lower bound on the contribution to the mixer noise is $T_M^Q \approx h\nu/k$[19a]. At the microwave frequencies we used, the quantum noise is almost negligible, ~1K. At Terahertz frequencies, the quantum noise limit is not negligible. T_M^Q = 120K at 2.5 THz. Since the measured mixer noise of Nb HEBs is much greater than T_M^Q, we believe that reducing the two thermal contributions, by use of Al HEBs, will reduce T_M. This should hold true even for more advanced noise theories. The mixer noise temperature at 30 GHz due to thermal sources is predicted to be ~8 K by scaling the best results obtained with Nb at 20 GHz by T_c.

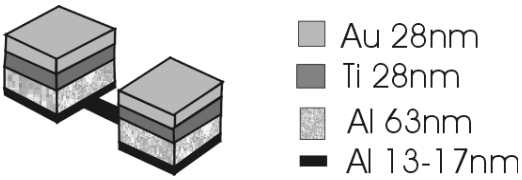

Fig. 2: Device geometry

II. Devices

The devices consist of a thin, narrow Al microbridge with dimensions d=13-17nm, W=0.1μm, and L=0.2-1μm, where d,W, and L are the thickness, width, and length, respectively. Thick contacts consist of a tri-layer of Al, Ti, and Au with thickness ~ 68nm, 28nm, 28nm respectively on top of the thin Al film. To avoid the formation of an oxide interface layer between the thin Al in the microbridge and the contact pads, both structures are metallized in the same deposition cycle using a double angle evaporation process. The fabrication details can be found in Ref. 20. Fig. 2 gives an illustration of the device geometry, and the device parameters are summarized in Table I.

The superconducting transition temperature of the Al microbridges in zero field ranged from ~ 1.5-2.4 K depending on length and resistivity. The contact pads are a combination of normal and super-

conducting metals, and have a transition temperature which is lower than that of the microbridge, with $T_{c,contact\ pads} \approx 0.6\text{-}1.0K$. For tests below $T_{c,contact\ pads}$ a perpendicular magnetic field is applied to suppress the superconductivity in the contact pads. The resistivity of the microbridge is significantly higher than that of the contact pads. The upper critical field of the microbridge is thus several kOe higher than that of the contact pads.[21]

The smallest magnetic field in which no signs of Josephson effects are observed is chosen as the operating field. Typically, this operating magnetic field is less than half of the upper critical field of the microbridge.

III. Experimental Setup

The devices are mounted on the cold stage of a variable temperature ^{3}He cryostat. The bath temperature was varied from 0.25-1.6K for the mixing experiments, and up to 40K for Johnson noise calibrations and other measurements. A schematic of the measurement setup is shown in Fig. 3.

Microwave signals are applied using the internal synthesized generator of a HP8722D vector network analyzer (0.05-40 GHz) and an Avantek YIG Oscillator (26.5-40 GHz).[22] A waveguide high-pass filter is used to remove noise from the HP8722D in the ⩽ 1 GHz range. The RF and LO signals are combined at room temperature via a coaxial direction coupler. A cold (4K) directional coupler is used to feed the RF/LO signals into the mixer block, and to couple out the IF signal. The mixer block uses a coaxial-microstrip transition to couple to the device.

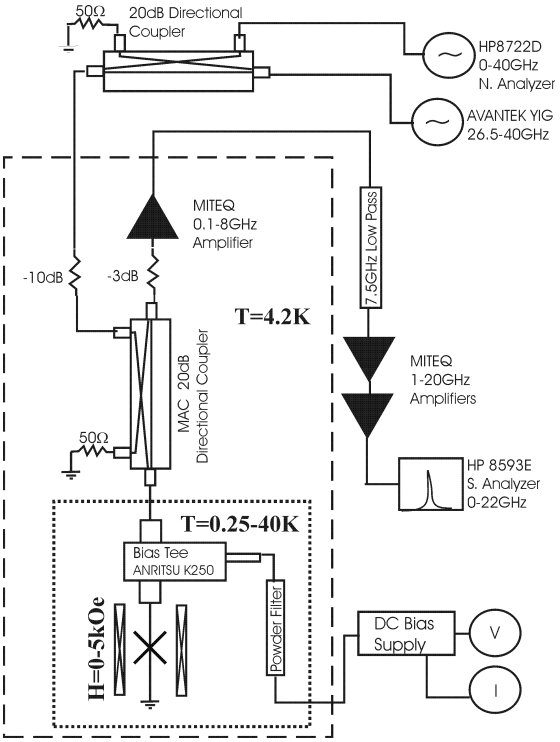

Fig. 3: Schematic of Measurement Setup

The IF amplifier chain consists of three broadband Miteq HEMT amplifiers. The first IF amplifier is immersed in liquid ^{4}He close to the device. By measuring the Johnson noise output of the HEB in the normal state as a function of bath temperature, the gain and noise temperature of the IF chain is obtained.

The output noise at IF = 1.20-1.25 GHz from the device is measured using a room temperature Shottky diode detector. The conversion efficiency at the same IF is used to calculate the mixer noise.

IV. Results

A. I-V Curves and R vs. T

I-V curves of device C in the absence of an external magnetic field are shown in Fig. 4. At temperatures ~0.6K and below, the small series resistance pre-

sent is that of the cables and microstrip line used in a two point measurement of the resistance.

When the contact pads are in the normal state, a significant resistance (~0.25 R_n - 0.5R_n depending on microbridge resistivity and length) exists even at temperatures well below T_c of the microbridge. For example, in device D, the transition temperature of the Al microbridge is ~2.4K and that of the contact pads is ~0.6K (see Fig. 5). At temperatures just below 2.4K where the superconducting energy gap is small, the observation of resistance can be explained due to charge imbalance effects.[23,24] However, at 0.6K ($t=T/T_c=0.25$) and at small voltages, nearly all of the single electrons incident on the N-S boundary should be converted to Cooper pairs via Andreev reflection.[23] Yet we observe a large finite resistance (Fig. 6). Dividing this observed resistance by the normal state resistance and multiplying by the length of the microbridge gives us the effective length of the resistive area in the microbridge.

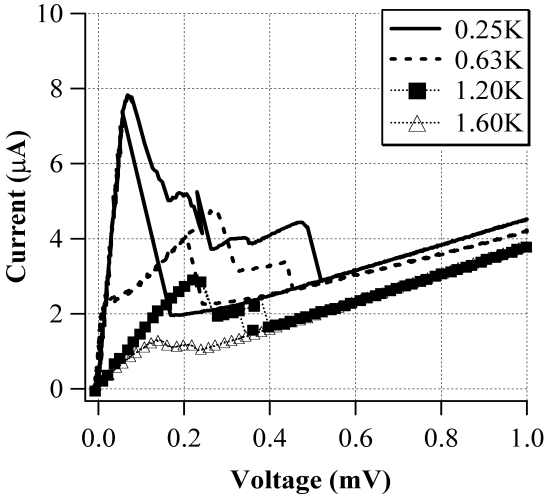

Fig. 4: I-V Curves for device C for bath temperature 0.25-1.6K. H=0.

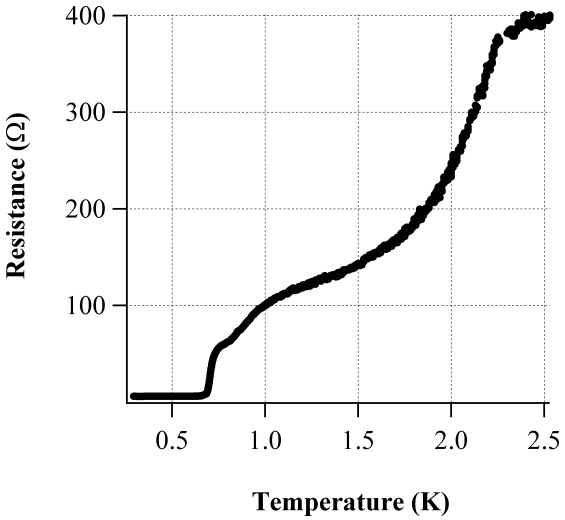

Fig 5: R vs. T of device D, H=0. The IV curves of thus device are like those of device C, Fig. 4.

Comparing this length to the superconducting coherence length, determined by upper critical field measurements, we see that the length of the resistive region is several coherence lengths in size.

One batch of devices has been manufactured without thick Al in the contact pads. The contact pads in this case are always in the normal state in the temperature regime used. Measurements on these devices also indicate that a large resistance remains down to the lowest temperature measured.[25] Measurements of R vs. T for device A are shown in Fig. 6 in an external magnetic field. The R vs. T for the devices with normal contact pads look very similar to Fig. 6, in which the superconductivity of the contact pads is suppressed in a magnetic field. The resistance depends only weakly on the bath temperature below 0.5K and appears to remain finite even as $T\rightarrow 0$. In the limit of zero temperature, when measuring resistance with a small excitation current, there should not be any resistance. We do not understand this low temperature resistance.

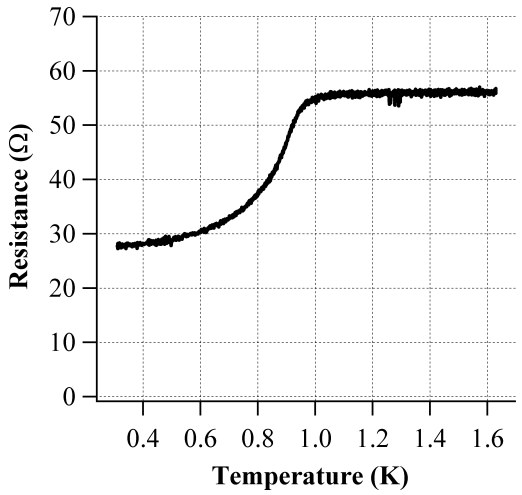

Fig 6: R vs. T of device A. H=1.2kOe.

Extrapolating the R vs. T dependence given in Fig. 6 to T=0, for example gives us a finite resistance, of larger value R_n ($6\xi/L$). For example, $\xi(0.25K)$=50nm for device A. The measured resistance at low bias voltages is 0.5 R_n, corresponding to a length of 6 $\xi(T)$.

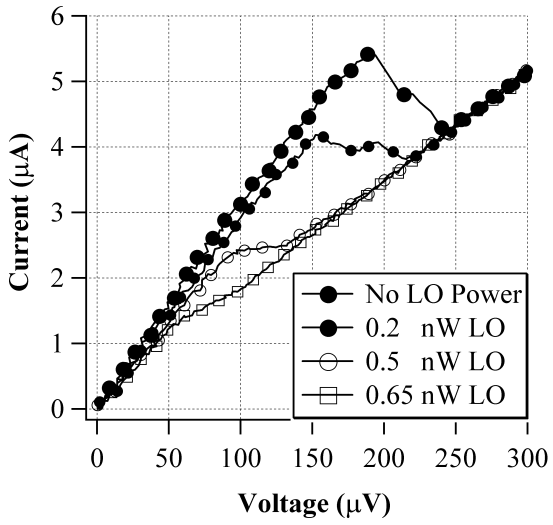

Fig. 7: I-V curves as a function of LO power. H=1.2kOe for Device A. T=0.25K

Additional features which may be due to phase-slip centers are also present in the I-V characteristics. It is not clear what will be the nature of these phase-slip structures at low temperatures in our device geometry. Further investigation is needed. Mixing is observed when biasing the device at low voltages, where the device is partly resistive at 0.25 to 0.5 R_n as discussed above, and when biasing the device at higher voltages, above the "kink" in the I-V curve (see Fig. 8). This "kink" is likely associated with the critical current of the microbridge. For P_{LO}=0.5nW, shown in Fig. 7, this kink occurs between 100 and 140μV, and the "high voltage" region is for larger voltages. The response observed at these higher bias voltages is hereafter termed the "resistive state" response. Though mixing at low bias voltage also may be promising, only the resistive state response is discussed in this work, as the conversion efficiency is better.

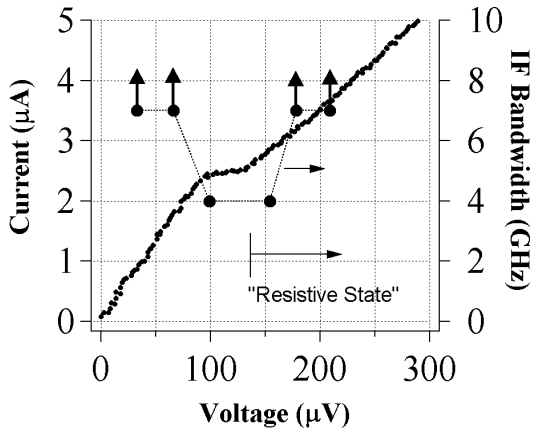

Fig. 8: IF bandwidth vs. bias voltage. The solid black line is the pumped I-V curve. The arrows indicate a bandwidth greater than measurement limit of this setup. Device A. T=0.25K.

B. IF Bandwidth

IF bandwidth depends on the bias point. For higher bias voltages in the resistive branch of the I-V curve (above 160 μV in Fig 8.), the IF bandwidth increases. Accompanying the increase in bandwidth is a sharp decrease in conversion efficiency. The best conversion in the resistive state is seen when biasing on the section of the resistive branch of the I-V curve just above the kink where it connects to the lower voltage branch, 140μV in Fig. 8. The IF signal was examined carefully to ensure that no sideband generation was observed for the data reported here. Sideband generation is seen for unstable bias points, where the dc differential resistance is negative.

The application of a magnetic field seems not to affect the bandwidth in the resistive state. For example, the IF bandwidth was measured at the lowest bath temperature with an applied magnetic field, and at temperatures above the transition temperature of the contact pads without a magnetic field. The two bandwidths coincide. The conversion efficiency measured at the lower bath temperature is slightly better.

In Fig. 9, a comparison is made between the measured IF bandwidth and the value predicted from a calculation of the diffusion time using Eq. 5, with $f_{-3dB} = 1/(2\pi\tau_{eff})$. The bias points considered in determining the IF bandwidth were the ones which gave the maximum conversion efficiency in the resistive state. We can see good agreement with the prediction for a diffusion-cooled mixer.

C. Optimum LO Power

The LO power used in the mixing experiments is in the range of ⩽ 1.0 nW delivered to the mixer block. Values of the conversion efficiency and mixer noise are presented as a function of LO power in Fig. 10. The mixer noise temperature is calculated from the output noise of the device and the conversion efficiency: $T_m(DSB)=T_{output}/2\eta$. The LO power needed for optimum conversion efficiency is approximately the same value that gives the best noise performance. Experimentally this is the case since the output noise is slowly varying with bias voltage and thus the dominant factor in determining the voltage dependence of the mixer noise is the conversion efficiency.

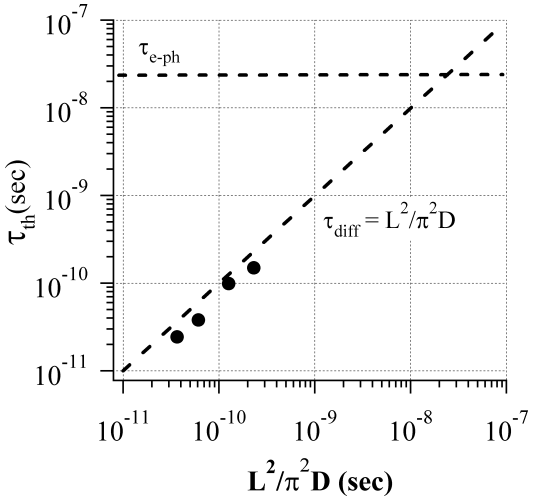

Fig. 9: IF Bandwidth: Measured & Predicted. The electron-phonon inelastic time is calculated from Ref. 8 for T=1.6K. The vertical axis is the measured relaxation time, where τ_{th} is determined experimentally using $\tau_{eff}=(2\pi f_{-3dB})^{-1}$ and Eq. 5. Data points are for devices B,A,D,C starting with the smallest time.

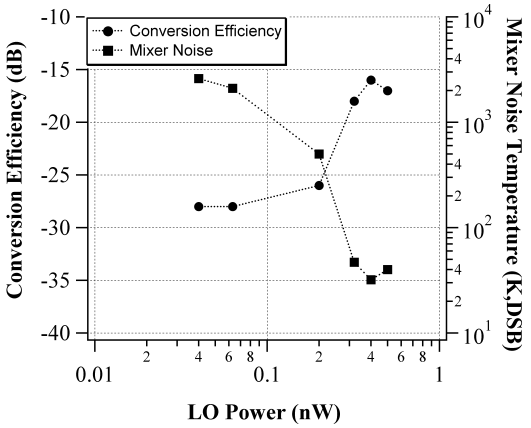

Fig. 10: Conversion Efficiency & Mixer Noise Temperature vs. LO Power. Device D. T=0.25K.

The term "optimum" will therefore be used to describe the situation when the device is nearly optimized for both mixer noise and conversion efficiency. The magnitude of the LO power is in quantitative agreement with the prediction in section I (Fig. 10).

Measurements of the temperature dependence of the optimum LO power were also made (Fig. 11). The temperature dependence is in agreement with the relation presented in Eq. (3).

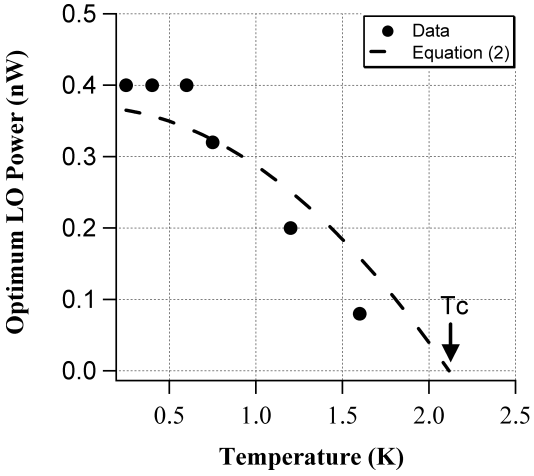

Fig. 11: LO Power vs. Temperature. Device D.

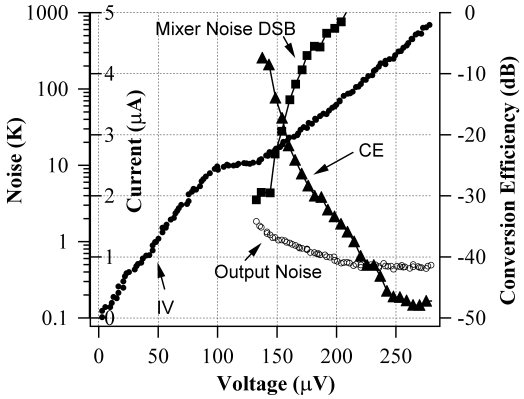

Figure 12: Conversion Efficiency, Output Noise, and Mixer Noise vs. Bias Voltage for Device A. T=0.25K. H=1.2kOe.

D. Mixer Noise

In Fig. 12, the dependence of mixer noise and of conversion efficiency on bias voltage is shown for device A, using $T_m=T_{out}/2\eta$. The minimum of the mixer noise temperature is ~4 K for device A. At the LO frequency used, this is ~ 3 hν/k. This mixer noise temperature is somewhat lower than predicted by simply scaling Nb data at 20 GHz according to T_c. The mixer noise temperature with a 20 GHz LO in Nb HEBs was ~ 120 hν/k in the case with a finite critical current, but 33 hν/k when the critical current was fully suppressed by P_{LO}.[16]

By looking at the dependence of the output noise on IF, Burke et al in Ref. 2 were able to separate the thermal fluctuation noise and Johnson noise components of the output noise. At zero intermediate frequency the output noise should be a combination of the thermal fluctuation noise and Johnson noise. Well above the rolloff frequency of the thermal fluctuation noise, the dominant noise should be Johnson noise. The values obtained for the "Johnson noise" contribution to the output noise were

output noise were several times larger than calculated for Johnson noise at the transition temperature of the Nb HEB, ~ 5.5K. The origin of this excess noise for Nb was not explained. For the Al HEBs, the total output noise is consistent with thermal fluctuation and Johnson noise contributions with Johnson noise of the magnitude expected for $T \sim T_c$.

The noise we reported above used an applied magnetic field. The output noise is less than the H=0 case. IV curves in a magnetic field, at bias voltages >1mV, do not exhibit excess current. At the same voltages, in zero field, the differential resistance is equal to R_n, but there is excess current: $I > V/R_n$. This implies that the contacts are still superconducting even though the bridge is in the normal state. The experimental correlation suggests that the additional output noise observed in zero field is correlated with the existence of superconductivity in the contact pads.

When pumped at microwave frequencies, the excess current still remains. Pumped IV curves where the superconductivity in the edges of the microbridge is suppressed by radiation at 618 GHz[26] do not show excess current. Measurements of the output noise in a magnetic field with LO power at 30 GHz agree with those at 618 GHz in zero field.[26]

The IV curves for the Nb devices show similar behavior in terms of excess current. Devices pumped at 20GHz show excess current. It is possible that the additional output noise observed at 20 GHz is due to the existence of superconductivity in the Nb areas underneath the thick Au contacts, like the case of Al microbridges.

V. Mixer Performance: Experiment and Theory

In this section we compare measured mixer performance with that predicted by theory. The conversion efficiency, output noise, and IF bandwidth can be calculated from thermodynamic considerations based on the device operating parameters – the dynamic resistance, bias current, temperature, thermal conductance, LO power, and the derivative of resistance with temperature.[19,27-29] A summary of these formulas is presented in Ref. 29, and are repeated here.

The conversion efficiency is defined as the ratio of the output power at the IF divided by the input power at the RF. The frequency dependent single-sideband (SSB) conversion efficiency is given by

$$\eta(\omega) = \frac{2R_L}{(R+R_L)^2} P_{LO} \left(\frac{I_{DC}\left(\frac{dR}{dT}\right)}{G_{eff}} \right)^2 X \quad \frac{1}{1+(\omega\tau_{eff})^2} \qquad (4)$$

where P_{LO} is the LO power, R is the device resistance, G_{eff} is the effective thermal conductance, I_{DC} is the device bias current, and ω is the IF. The resistance R is defined as the dc voltage divided by the dc current. R_L is the load resistance – which in this case is the 50Ω input impedance of the first stage IF amplifier. Electro-thermal feedback effects which tend to modify the thermal conductance and time constant are included using the factor α.

$$\tau_{eff} = \tau_{th} / (1-\alpha), \qquad (5)$$

$$G_{eff} = G(1-\alpha), \qquad (6)$$

Table II: Mixer parameters: Experiemtal results and theoretical predictions.

	Experiment						Theory			
Device	**Rn (Ohm)**	**T_b (K)**	**IF BW (GHz)**	**η (dB)**	**T_{out} (K)**	**$T_{mix}= T_{out}/2\eta$ (K,DSB)**	**IF BW (GHz)**	**η (dB)**	**T_{out} (K)**	**$T_{mix}= T_{out}/2\eta$ (K,DSB)**
A	52	0.25	4	-8	1.3	4	2.5	-9	1.3	5
B	145	1.2	6	-27	…	…	5	-22	…	…
C	260	1.2	1.2	-33	…	…	0.8	-31	…	…
D	387	0.25	2	-16	1.6	32	1.7	-15	1.6	27

$$\alpha = \frac{I_{DC}^2 \, dR/dT}{G}\left(\frac{R_L - R}{R_L + R}\right) \qquad (7)$$

The parameter α can be determined from the pumped I-V characteristics using the following relation from Ref. 28:

$$\alpha_0 = \frac{I_{DC}^2}{G}\frac{dR}{dT} = \frac{\frac{dV}{dI} - \frac{V}{I}}{\frac{dV}{dI} + \frac{V}{I}}. \qquad (8)$$

The thermal conductance G can be estimated from the device resistance and the Wiedemann-Franz relation.[5]

The output noise is modeled as consisting of thermal fluctuation noise and Johnson noise. The Johnson noise component of the output noise temperature is taken to be equal to the average electron temperature θ, which can be estimated from the R vs. T characteristic and the device resistance at the operating point; θ = T_c. The frequency dependent output noise due to fluctuations in the electron temperature is given by

$$T_{TF}(\omega) = \left(I_{DC}\theta\frac{dR}{dT}\right)^2 \frac{1}{RG_{eff}(1-\alpha)} \qquad (9)$$

$$X \quad \frac{1}{1+(\omega\tau_{eff})^2}\frac{4RR_L}{(R+R_L)^2}$$

In Table II we present the experimental and predicted values for mixer parameters for near optimum operating conditions. The conversion efficiency and output noise are calculated from the relations given above. The IF bandwidth is estimated from Eq. (1) and Eq. (5). We see good agreement between theoretical predictions and experimental results.

We can calculate the conversion efficiency and output noise using the formulas above for different bias voltages and different LO powers. These calculations are in also good agreement with experimental data. As an example, in Fig. 13, we show how the measured conversion efficiency for device A compares with theoretical prediction.

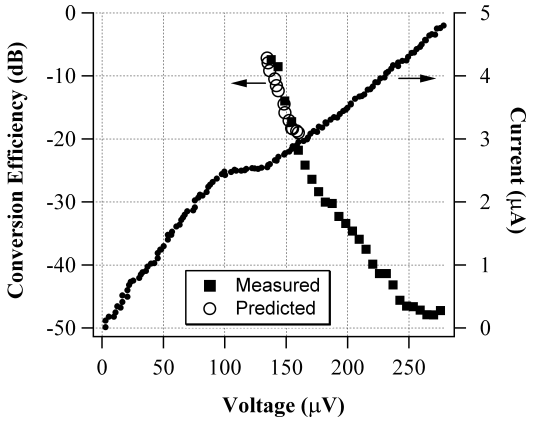

Fig. 13: Measured and predicted conversion efficiency. Device A. T=0.25K.

For operation at Terhaertz frequencies, we can empirically estimate the mixer noise from the 30 GHz data by scaling the microwave data linearly with frequency. At 30 GHz we measure $T_m \sim 3\ h\nu/k$. If the same sensitivity is present at 2.5 THz, the mixer noise is then predicted to be $T_m \sim 360$K. As a check, we can compare with measurements at 618 GHz. The output noise of Al HEBs measured at 618 GHz ranges from 1-2K. The conversion efficiency under the same conditions is estimated to be ~ -21 dB.[26] The calculated mixer noise temperature is thus $T_m \sim$ 125 K, DSB. From the 30 GHz data, one would predict $T_m \sim 90$K for 618 GHz. So our estimates seem to be consistent with the existing data. These estimates do not include rf submillimeter coupling losses which are present in any receiver. At 30GHz, coupling losses are negligible

VI. Conclusions

Results for mixing with Al HEBs at microwave frequencies are very good. The IF signal bandwidth scales with device length and diffusivity as predicted in the diffusion cooling model, Eq. (1a). The LO power needed for mixing scales approximately linearly with T_c. The measured mixer noise is somewhat lower than that predicted by scaling Nb HEB results. The measured IF bandwidth and optimum LO power are in good agreement with lumped element predictions.

The diffusion time in the these devices is comparable to or larger than the inelastic electron-electron time[8] τ_{ee}. Recently, predictions were made for HEBs which are very short $L \ll (D\,\tau_{ee})^{1/2} = L_{ee}$ in which thermalization via electron-electron interaction would be absent in the microbridge. Such a short device would have large LO power requirements in the μW range.[30] These predictions were made for an operating frequency of 2.5 THz. For device A (L=600nm), L_{ee} = 600nm for $T=T_c$. The other devices have a larger sheet resistance and are longer than the inelastic electron-electron length. Thus, our devices are not in the regime treated by Ref. 30. In any case, measurements at 30 GHz cannot address this issue, since 30 GHz is below the gap frequency; $\nu_{gap} \sim$ 110 GHz at T=0 and H=0 for device A. However, measurements at 618 GHz could speak to this issue. Results at JPL[26] on a device comparable to our device A show that $P_{LO} \leqslant 10$nW. We emphasize that the device studied at JPL also had $L > L_{ee}$, as proposed in the original theory paper on diffusion cooling.[5] If we scale the predictions in Ref. 30 as the frequency squared, the expected LO power for this bridge with $L \geq L_{ee}$, is still substantially less than that predicted for $L \ll L_{ee}$.

Currently, a major design issue for space-borne application of HEB mixer receivers is the availability of an appropriate LO source. Molecular lasers are heavy and need high-power sources. A CW solid state generator was demonstrated recently[31] using a p-Ge laser biased at relatively low bias voltages compared with pulse mode voltages. However, it is unclear if is it possible to get a narrow enough spectral line (~1MHz) with the p-Ge laser. The other real possibilities at present are photomixer sources and multipliers A successful traveling-wave THz photomixer has been shown to have an output power of at least ~ 10nW above 1 THz.[32] This is not enough for mixing with Nb HEBs. But our results for the optimum LO power for Al HEB mixers indicate that there is real possibility for integrating a

THz Al HEB mixer with such a photomixer.

Acknowledgements

The authors thank Prof. R.J. Schoelkopf for use of equipment in his lab, and Rich Lathrop for help in the early experiments. This research was supported by the NSF and NASA Office of Space Science. Funding for I.S. was provided by a NASA Graduate Student Fellowship.

References

[1] B.S. Karasik and W.R. McGrath, in *P Proceedings of the 9th International Symposium on Space Terahertz Technology,* edited by W.R. McGrath (Pasadena, CA, 1998), pp. 73-80; D.E. Prober (unpublished).

[2] P.J. Burke, R.J. Schoelkopf, D.E. Prober, A. Skalare, B.S. Karasik, M.C. Gaidis, W.R. McGrath, B.Bumble, and H.G. LeDuc, J. Appl. Phys. 85, 1644 (1999).

[3] R. A. Wyss, B.S. Karasik, W.R. McGrath, B. Bumble, H. LeDuc, in *Proceedings of the 10th International Symposium on Space Terahertz Technology,* edited by T. Crowe and R.M. Weikle (University of Virginia, Charlottesville, VA, 1999), pp. 215-228; B.S. Karasik, M.C. Gaidis, W.R. McGrath, B. Bumble, H.G. LeDuc, Appl. Phys. Lett 71, 1567 (1997).

[4] E. Gerecht, C.F. Musante, H. Jian, Y. Zhuang, K.S. Yngvesson, J. Dickson, T. Goyette, J. Waldman, P.A. Yagoubov, G.N. Gol'tsman, B.M. Voronov, and E. M. Gershenzon, in *Proceedings of the 10th International Symposium on Space Terahertz Technology,* edited by T. Crowe and R.M. Weikle (University of Virginia, Charlottesville, VA, 1999), pp. 200-207.

[5] D.E. Prober, Appl. Phys. Lett. 62, 2119 (1993).

[6] J.M. Gordon and A.M. Goldman, Phys. Rev. B. 34, 1500 (1986).

[7] Y. Bruynserade, M. Gijs, C. Van Haesendonck, and G. Deutscher, Phys. Rev. Lett. 50, 277 (1983).

[8] P. Santhanam and D.E. Prober, Phys. Rev. B 29, 3733 (1984).

[9] B. Shinozaki, T. Kawaguti, and Y. Fujimori, J. Phys. Society Japan 61, 3678 (1992)

[10] E.M. Gershenzon, G.N. Gol'tsman, V.D. Potapov, and A.V. Sergeev, Solid State Commun. 75, 639 (1990)

[11] M. Park, K.R. Lane, J.M Parpia, M.S. Isaacson, J. Vac. Sci. Technol. A 13, 127 (1995).

[12] C. Kittel, *Introduction to Solid State Physics, Seventh Edition* (John Wiley & Sons, Inc., New York, 1996), pp. 158-159.

[13] W. Liniger, J. Low Temp. Phys. 93, 1 (1993).

[14] C.C. Chi, P. Santhanam, S.J. Wind, M.J. Brady, and J.J. Bicchigano, Phys. Rev. B 50, 3487 (1994).

[15] This calculation assumes that the microbridge is connected with contact pads made of the same material as the microbridge, but in the normal state.

[16] P.J. Burke, Ph.D. thesis, Yale University, 1997, available from authors.

[17] J. Schubert, A. Semenov, G. Gol'tsman, H.W. Hubers, G. Schwab, B. Voronov, E. Gershenzon, in *Proceedings of the 10th International Symposium on Space Terahertz Technology,* edited by T. Crowe and R.M. Weikle (University of Virginia, Charlottesville, VA, 1999), pp. 190-199.

[18] A magnetic field was not used in measurements made at 618 GHz. Superconductiivty in the edges of the microbridge was suppressed using LO power. This might account in part for the higher LO power used.

[19] B.S. Karasik and A.I. Elantiev, Appl. Phys. Lett 68, 853 (1996).

[19a] C.M. Caves, Phys. Rev. D, 26, 1817 (1982).

[20] P.M. Echternach, H.G. LeDuc, A. Skalare, W.R. McGrath, in *Proceedings of the 10th International Symposium on Space Terahertz Technology,* edited by T. Crowe and R.M. Weikle (University of Virginia, Charlottesville, VA, 1999), pp. 261-268.

[21] Applying a magnetic field suppresses the thick contact pads. The thin Al layer underneath is proximitized normal.

[22] To calibrate out any resonances in the RF input line, the RF power needed to suppress the IV curve to the same state was measured for the frequencies used. The relative difference was then used in the mixing experiments to adjust the input power so that the RF power remained constant.

[23] G.E. Blonder, M. Tinkham, and T.M. Klapwijk, Phys Rev B 25, 4515 (1982).

[24] D. Wilms Floet, J.J.A. Baselmans, and T.M. Klapwijk, Appl. Phys. Lett. 73, 2826 (1998).

[25] P.M. Echternach (unpublished).
[26] A.Skalare et al, in *Proceedings of the 11th International Symposium on Space Terahertz Technology,* edited by J. West (U. Michigan, Ann Arbor, MI, 2000); A. Skalare private communication).
[27] F. Arams, C. Allen, B. Peyton, and E. Sard, Proc. IEEE 54, 612 (1966).
[28] H. Ekstrom, B. Karsik, E. Kollberg, and K. Yngvesson, IEEE Trans. Microwave Theory-Tech 43, 938 (1995).
[29] B. Karasik and A. Elantiev, in *Proceedings of the 6th International Symposium on Space Terahertz Technology,* edited by J. Zmuidzinas and G. Rebiez (Caltech, Pasadena, CA, 1995), pp. 229-246.
[30] A.D. Semenov and G.N. Gol'tsman, J. Appl. Phys 87, 502 (2000).
[31] Yu. P. Gousev, I.V. Altukhov, K.A. Korolev, V.P. Sinis, M.S. Kagan, E.E. Haller, M.A. Odnoblyudov, I.N. Yassievich, and K.A. Chao, Appl. Phys. Lett. 75, 757 (1999).
[32] S.Matsuura, G.A.Blake, R.A.Wyss, J.C.Pearson, C.Kadow, A.W.Jackson, and A.C.Gossard, Appl. Phys. Lett. 74, 2872 (1999).